American Academic Scientific Research Journal for Engineering, Technology, and Sciences
ISSN (Print) 2313-4410, ISSN (Online) 2313-4402
http://asrjetsjournal.org/

Simulation of Transonic Compressor Performance Deterioration Due to Sand Erosion

Nizar A. Qattan[a]*, Ali M. Al-Bahi[b], Belkacem Kada[c]

[a,c]*Aerospace Engineering Department, King Abdulaziz University, Jeddah 21589, Saudi Arabia*
[a]*Email: qattan.n@gmail.com*
[b]*Email: albahi@gmail.com*
[c]*Email: bkada@kau.edu.sa*

Abstract

Air sand erosion is a widely effecting phenomenon in GCC region, where a solid particle impacting on a wall surface causing catastrophic mechanical damage, the engine compressor operating in a particulate environment are subjected to deterioration of performance and life due to sand ingestion. In current paper we simulate and studied the sand erosion in such transonic compressors were flow rate, particle size and concentration were investigated to study particles distribution and erosion rate along the compressor blade. Result shows that particles concentration has the most significant effect on blade erosion rate where particles size has less effect among all other measured parameters. Surface deformation and roughness is in scope for further investigation.

Keywords: Airfoil deterioration; Compressor; Erosion; Rotor 37; Transonic.

1. Introduction

In previous study NASA Rotor 37, originally designed and evaluated by Reid and Moore [1], and used for CFD and experimental validation, Serval studies have been conducted to understand compressor blade erosion in the literature. Suzuki and his colleagues [2], numerically investigated the particle trajectories and change of flow field in a single stage axial flow compressor and reported that first impact holds dominance for major erosion. Later Suzuki and Yamamoto. [3] developed a three-dimensional sand erosion prediction code and concluded that major impact of particles is concentrated on leading edge and pressure side of the blade.

----

* Corresponding author.

Similarly, Reference [4] calculated erosion on the compressor surface. They also reported maximum erosion rate on pressure surfaces and impeller part of the compressor. Reference [5] proposed an algorithm to estimate the efficiency degradation of compressor utilizing the data from T700-GE-701C engine and using Kalmnan filter as estimator by feeding it input data from engine's sensors. They provided a tool to track performance variation to detect wear and erosion for compressor blades especially in sandy environments. Reference [6] analyzed performance loss in compressor caused blade erosion due to ingested particles in and compared the simulated results with mean line compressor performance model. They recorded 3-4 % reduction adiabatic efficiency under the combined effects of blade surface roughness and tip clearance caused by erosion. Lakshminarasimha and his colleagues [7] developed a model to determine the effects of erosion in multistage compressor reporting overall compressor performance and effect of erosion on a specific stage of compressor. They reported overall performance of compressor is highly affected by first stage of the compressor as compared with the rear stages.

In the current study, effect of the erosion on the performance of a transonic compressor's rotor has been investigated numerically. Where, transonic compressor rotor has been used for the first time for erosion effect on the compressor's performance. Flow in a transonic rotor is governed by a bow shock wave that could alter the erosion pattern that has been studied and reported in the above listed studies. Initially, computational model developed for the current study was validated against the experimental aerodynamic data produced and published by NASA. Later effect of the erosion was investigated on the compressor's rotor performance using different mass concentrations of the sand particle and various sand particle sizes.

1.1. Methodology

Initially a computational model was developed for the NASA rotor 37 and then was validated by comparing the numerical results with the experimental results. The compressor rotor has been designed by NASA as a low aspect ratio transonic inlet stage for a core compressor to study the effects of aspect ratio and loading level on the performance of speed stages. The rotor design pressure ratio is 2.106 at a mass flow rate of 20.19 kg/s with a measured choking mass flow of 20.93 kg/s. The relative Mach number at the inlet is 1.13 at the hub and 1.48 at the tip at the design wheel speed of 17,188.65 rpm, giving a nominal tip speed of 454 m/s. The rotor has 36 blades with an aspect ratio of 1.19, hub to tip ratio of 0.70, and a tip solidity of 1.288. The running tip clearance was estimated to be 0.356 mm (0.5% span). Geometrical model of the rotor 37 is shown in the Figure. 1.

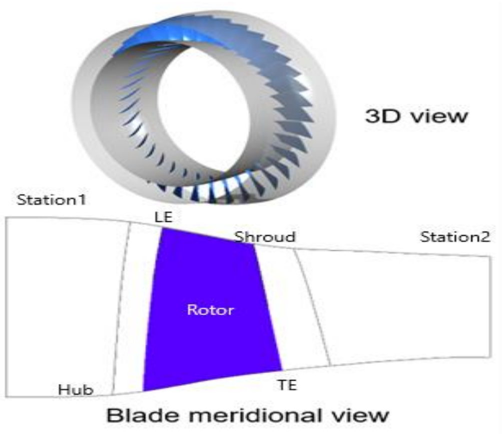

Figure 1: Geometry of the NASA rotor 37

1.2. Erosion model

Impact of the particles on the walls initiates wear and tear on the wall surface causing erosion on wall material which is a function of particle parameters, such as turbulent field, multiphase effects, effect of local flow cavities due to material removal and wall material properties. As per study of Hutchings [8], particle impact angle and velocity are major functions of erosion and suggested a relationship as;

$$E = kV_p^n f(\gamma) \tag{1}$$

Whereas E here is a dimensionless mass, V_p is particle velocity and $f(\gamma)$ is angle of impact in radians. Meanwhile value of n ranges from 2.3 to 2.5. Finnie. [9] suggest a model based upon his study for ductile materials for the value of $n = 2$, is adopted to predict the wear in current study as Finnie model relates with kinetic energy of particles.

$$E = kV_p^2 f(\gamma) \tag{2}$$

In Equation. 2

$$\begin{aligned} f(\gamma) &= \frac{1}{3}cos^2\gamma \qquad && if\ tan\,\gamma > \frac{1}{3} \\ f(\gamma) &= sin\,2\gamma - 3\,sin^2\gamma && if\ tan\,\gamma \le \frac{1}{3} \end{aligned} \tag{3}$$

1.3. Computational mesh

The discretization of rotating domain is performed using hexahedral mesh elements in ANSYS Turbo-grid console. Mesh of the rotor geometry is shown in the Figure. 2. One ratio one node connection is ensured at the interface boundaries. To minimize the probability of interpolation losses at the interface, same meshing topology was adopted for rotating and stationary domains [10]. Topology employed for the computational domains is based on O-grids [10], [11].. The topology of the mesh and distribution of the nodes are shown in

Figure. 2

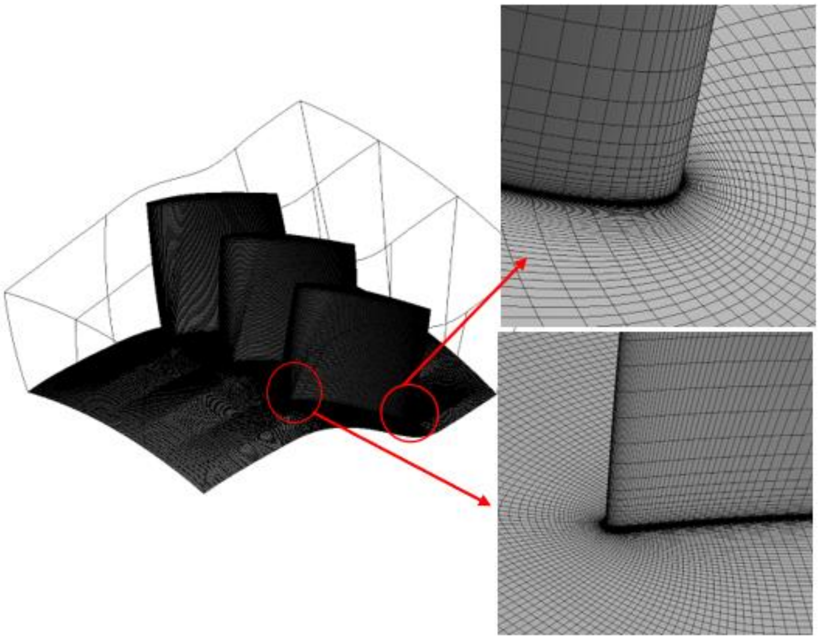

Figure 2: Mesh distribution on the hub and blade

1.4. Boundary conditions and validation

To simulate the rotor 37 model, one passage was modeled using periodic conditions to reduce the computational time and resources. A very robust set of boundary conditions were imposed in the inlet and outlet of the computational domain i.e., total pressure inlet and static pressure outlet conditions. While rotational periodicity was imposed on the bounding surfaces of the passage in the θ direction as shown in the Figure. 3. No slip wall conditions were applied on the rotor, hub and shroud wall. Shroud wall was modeled as stationary wall while rotor and hub walls were modeled as rotating walls along with the computational domain rotating at 17188.65 RPM.

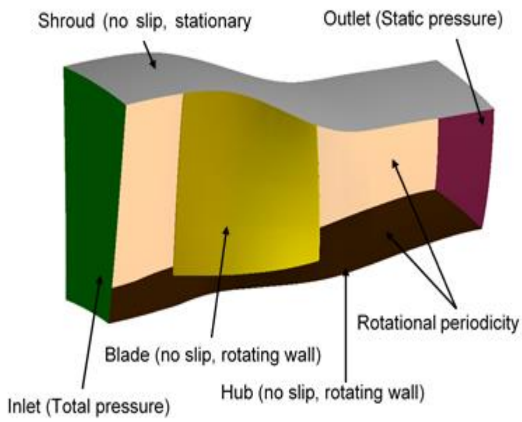

Figure 3: Details of the imposed boundary conditions

Comparison of the numerical and experimental results shown in the Table 1, while comparison of the pressure ratio profile has been shown in the Figure. 4. Results suggest that numerical results are quite close to the experimental results and developed computational model can be used for the further erosion analysis.

Table 1: Comparison of the numerical and experimental results

Pressure ratio			Efficiency			Mass flow rate		
Experimental	Numerical	%Age difference	Experimental	Numerical	%Age difference	Experimental	Numerical	%Age difference
2.11	1.98	-5.98	0.92	0.89	3.26	20.19	19.97	1.09

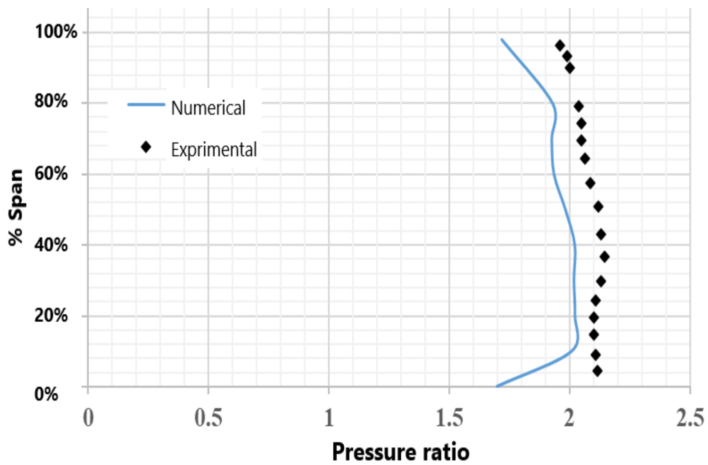

Figure 4: Pressure ratio comparison between the experimental and numerical results at the exit plane

In order to investigate the effect of erosion rate on the performance of the transonic compressor rotor effect of the flow rate of air (m_a), particle mass concentration (m_P) and size (d_P) of the particles of the solid have been studied. Following Table 2 lists the different conditions under which erosion rate and effects of the erosion rates have been studied.

Table 2: List of the conditions studied

Mass flow rate of the air through all passages ($\dot{m}_a$) $[kg\ s^{-1}]$	Flow rate of the solid particles per passage ($\dot{m}_a$) $[kg\ s^{-1}]$	Particle diameter (d_p) $[\mu m]$
19.5	0.5	150
19.75	0.75	200
20.09	1.0	250
20.73	NA	NA
20.93	NA	NA
21.05	NA	NA

1.5. Results and conclusion

Figure. 5, shows Mach number contours on the turbo surface plotted corresponding to the different values of the span locations i.e., 5%, 25%, 50% and 75%. It could be noted for the all span locations, Mach number is higher than one in the baled passages near the blade leading edge. The supersonic flow in the blade passage initiates a bow shock wave that hits the high pressure side of the next blade causing flow separation in the downstream of the hitting point as it could be seen in Figure. 5. Comparison of the strength of the shock wave at different spans dictates that it increases with the increase in the value of the span number as tangential component of the velocity increase in the span wise diction. Figure. 6, shows contours of the erosion rate density on both high pressure and low pressure sides of the blades. It is obvious from the figure that erosion rate density on the low pressure side is very low in comparison with the erosion rate density on the high pressure side. Moreover, most affected areas on the high pressure side are either in the vicinity of the hub region or the shroud region. Highest values of the erosion rate density were found in tip region of the blade i.e., from 95% span to 100% span.

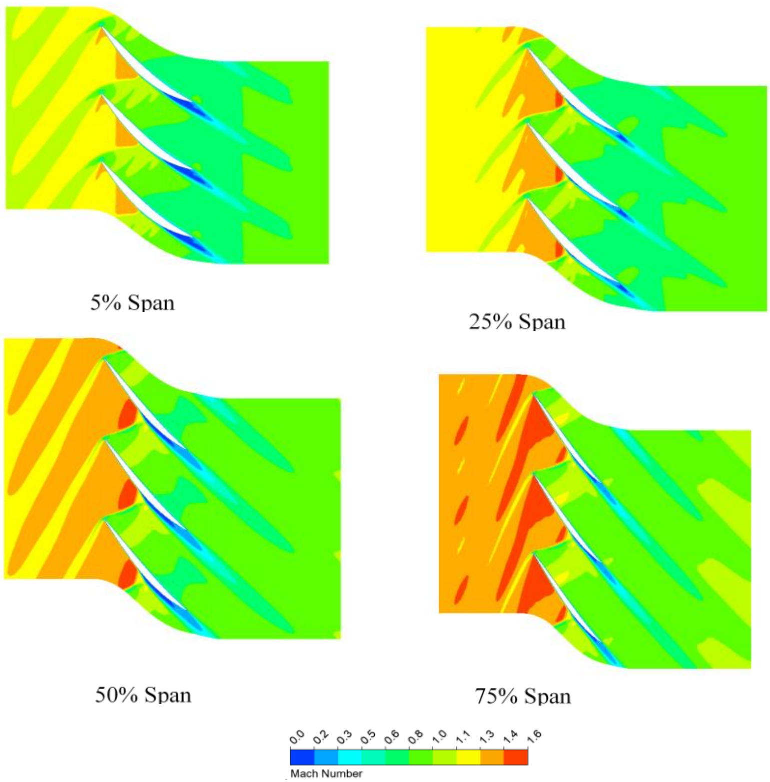

Figure 5: Mach no. contours using blade to blade view at different span locations

Detailed distribution of the erosion rate density at various span location corresponding to different flow rates of air i.e., $m_1 - m_6$, are shown in the Figure.7. Figure 7a show variation of the erosion rate density along the stream wise direction corresponding to minimum value of the air flow rate i.e. $m_1 = 19.5$ at various span location. It shows that highest convention of particle hitting the blade corresponding to 0% span and 25% is at the stream wise direction that ranges from 0.4-0.6. Whereas maximum value of the erosion rate density along with the concentration of the particles hitting the ground at 50% span were found maximum corresponding to stream wise location ranging from 0.1-0.3. On the other hand, at higher span locations i.e., 75% and 100% span, maximum values of the erosion rate density were found toward the trailing edge of the blade (stream location ranging from 0.75-1.0). Similar response could be seen for mass flow rate $m_2 = 19.74$ as clear form in Figure 7b. However, at higher flow rates i.e.,$m_3 - m_5$, maximum value of the erosion rate density for 100% span shifted towards the leading edge of the blade (stream wise locations ranging from 0.1-0.5). Whereas trends for the erosion rate density and collision rates at other span locations remains unchanged.

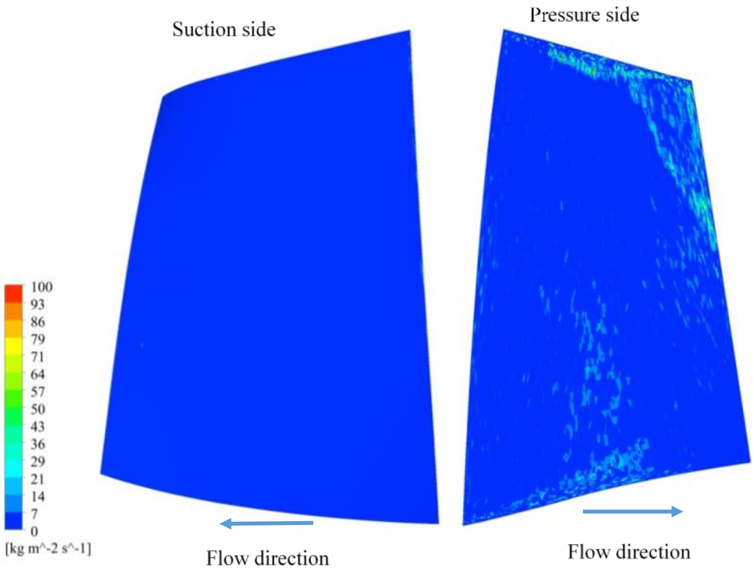

Figure 6: Erosion rate density contours plots on the suction and pressure sides

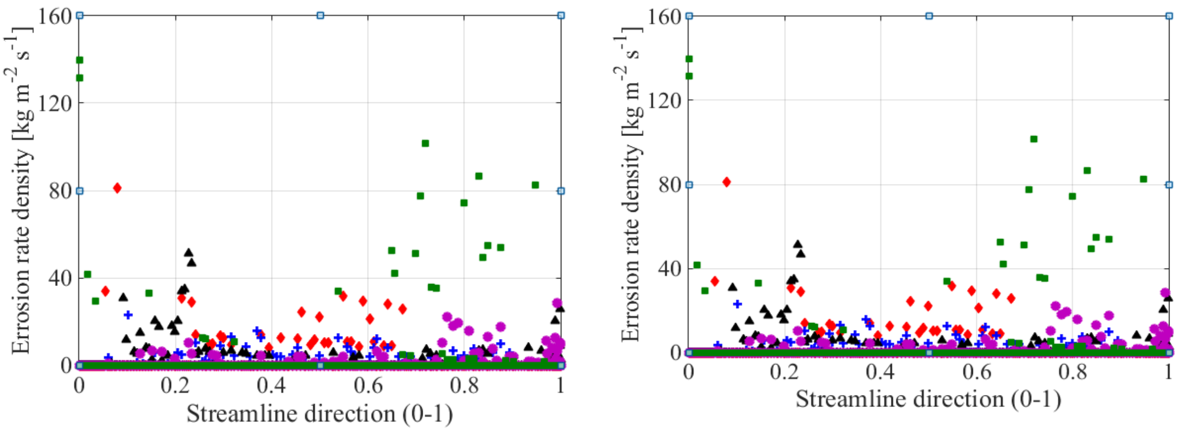

$a)\ m_a = m_1 = 19.5$ $b)\ m_a = m_2 = 19.74$

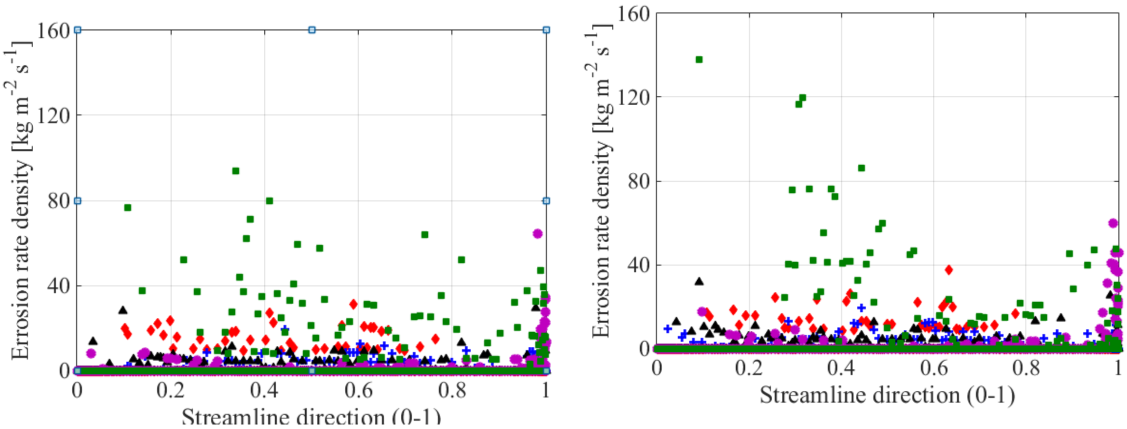

c) $m_a = m_3 = 20.09$ d) $m_a = m_4 = 20.73$

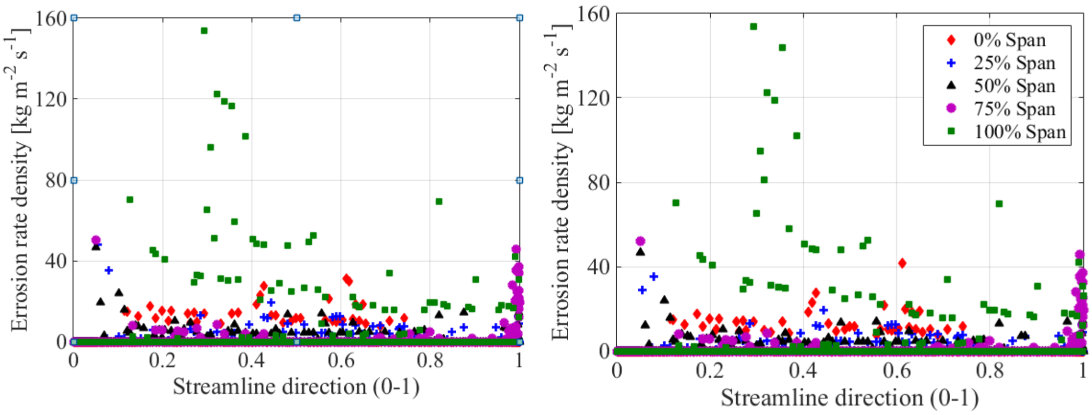

e) $m_a = m_5 = 20.93$ f) $m_a = m_6 = 21.05$

Figure 7: Erosion rate density distribution plotted at various span locations corresponding to the different mass flow rates air on the pressure side of the blade

Average values of the erosion rate density at different spans corresponding to the different values of the airflow rate are shown in the Figure. 8. It could be seen form the graph, for all air flow rates, average values of the erosion rate density decrease with span initially and later at higher span values it starts increasing with the increase in the blade span value. Heights values of the erosion rate density and averaged erosions rates density was found 160 $kg\ m^{-2}\ s^{-1}$ and 8 $kg\ m^{-2}\ s^{-1}$ respectively that corresponds to the maximum value of the air flow rate. Effect of air flow rate on the erosion rate density was found insignificant at lower span values while at higher span values i.e., 75% and 100%, effect of air flow rate on the erosion rate density is quite distinguishable. The difference between the minimum and maximum vales of the averaged erosion rate density at 75% span and 100% span were recorded as 101% and 88% respectively while corresponding difference was found only 17% at 0% span.

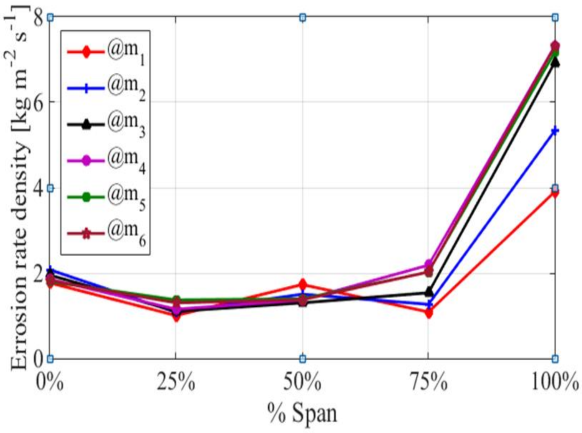

Figure 8: Average value of the erosion rate density distribution plotted at various span locations corresponding to the different mass flow rates air on the pressure side of the blade

Figure. 9 shows distribution of the erosion rate density along the blade stream wise direction for various span locations for different particle sizes. Comparison of the Figure.9a, 9b and 9c dictates the maximum value of the erosion rate density remains unchanged with the increase of particle size, however, the length of the blade over which its effect is concentrated increases with the increase in the value of the particle size. For example, for the particle size i.e., $dp = 150\mu m$, range of stream wise direction for which particles casing higher values of erosion rate density is 0.6 to 0.8. On the other hand, for $dp = 200\mu m$, the length of the blade effected by the higher erosion rate density values ranges form from 0.3-1 that encompasses the 70% of the blade length. For highest values of the particle size used in this study, i.e., $dp = 200\mu m$, effected length has increased to 90% of the blade length as higher values of the erosion rate densities could be seen in the range of stream wise location that ranges now from 0.1-1.0.

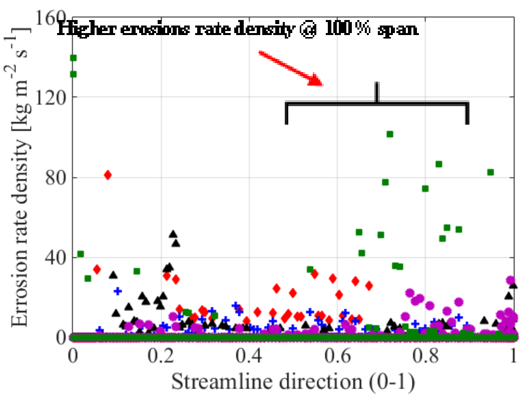

a) $d_P = 150\ \mu m$

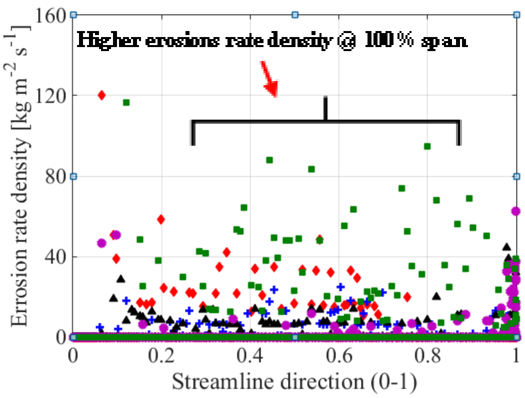

b) $d_P = 200\ \mu m$

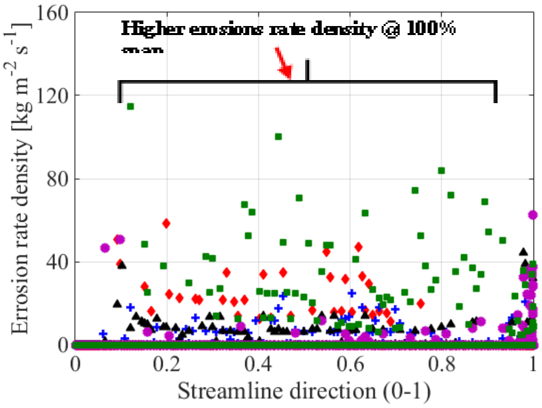

$c)\ d_P = 200$ µm

Figure 9: Erosion rate density distribution plotted at various span locations corresponding to the varied sizes of the sand particles on the pressure side of the blade

Above explained effect of the particle size on the erosion rate density could be further elaborated in terms of averaged values of the erosion rated densities over a specific span location. As the effected length of blade by higher values of erosion rate density increases with the increase in the value of the particle size with similar values of the maximum erosion rate density (as discussed above), average values of the erosion rate density for a certain span location must increase that is evident in Figure. 10. It is obvious from Figure. 10 that average values of the erosion rate density increase with the increase in the value of particle size at every span location. Increase in the value of erosion rate density with the increase in the value of d_P from $150\mu m$ to $250\mu m$ were computed as 77%, 99% and 49% at 0%, 50% and 100% span locations respectively.

Figure. 11 shows distribution of the erosion rate density along the blade stream wise direction for different span locations corresponding to the different mass flow rate values of the particles. The effect of the values of particle flow rate is same as the effect of the particle size as increase in the particle flow rate does not increase the value of the maximum erosion rate density values but only the effect length increased corresponding to every span location that increases the average value of the erosion rate density. Effect of particle flow rate on the average value of the erosion rate density is shown in the Figure. 12. It is obvious that average values of the erosion rate density increase significantly with the increase in the value of the particle flow rate at every span location. Increase in the value of erosion rate density with the increase in the value of m_P from 0.5 kg to 1.0 kg be computed as 88%, 129% and 102% at 0%, 50% and 100% span locations respectively. This shows effect of the particle's mass flow rate is higher on the erosion rate density in comparison with the effect of particle size on the erosion rate density.

American Academic Scientific Research Journal for Engineering, Technology, and Sciences (ASRJETS) (2022) Volume 90, No 1, pp 95-108

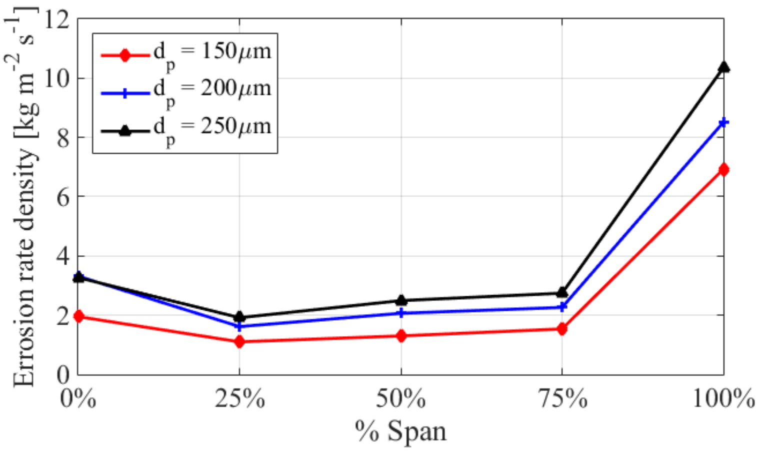

Figure 10: Average values of the erosion rate density distribution plotted at various span locations corresponding to the varied sizes of the sand particles on the pressure side of the blade

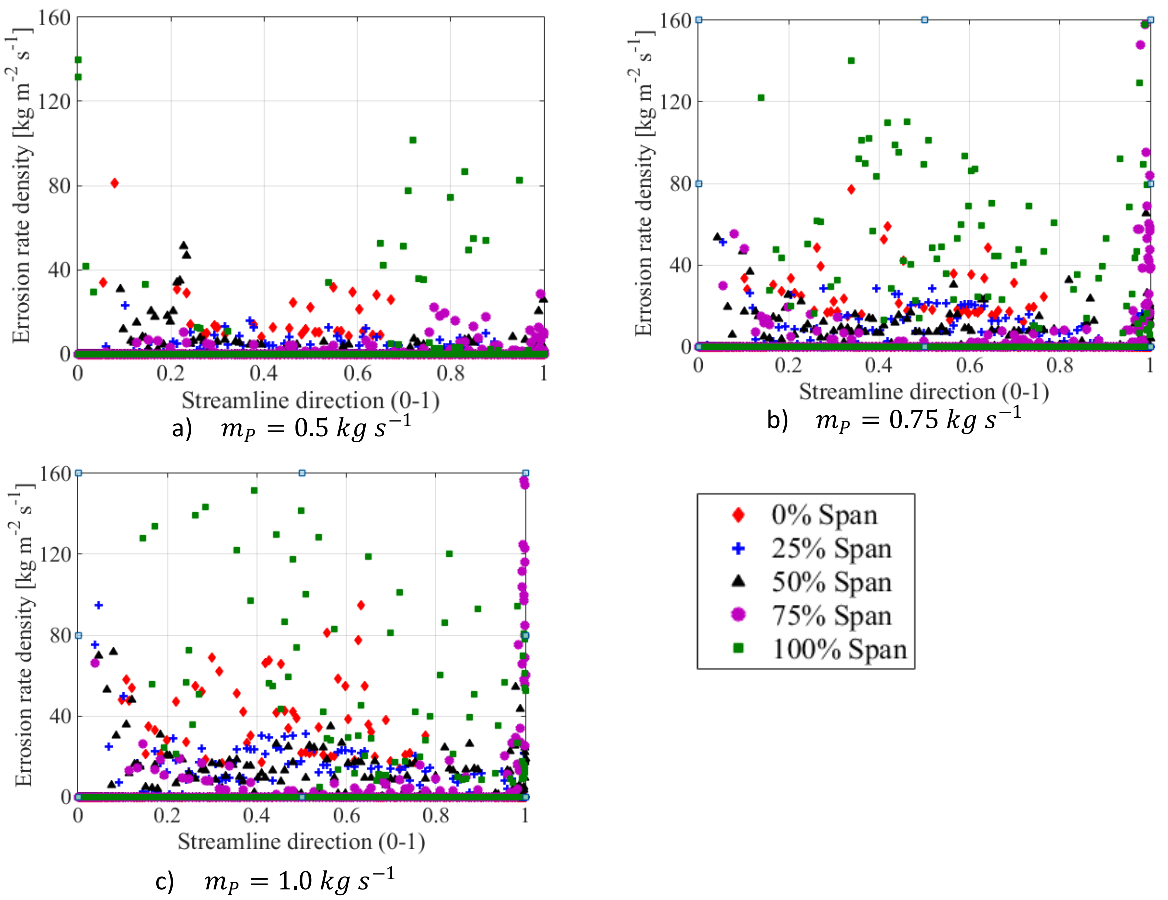

Figure 11: Erosion rate density distribution plotted at various span locations corresponding to the different mass flow rates of the sand particles on the pressure side of the blade

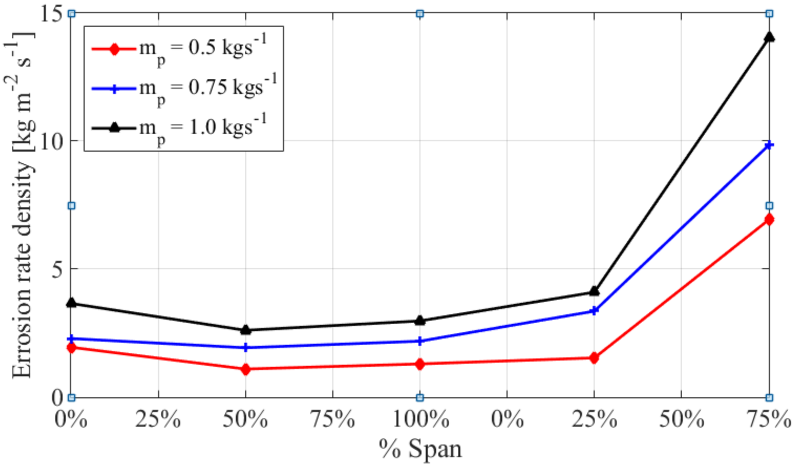

Figure 12: Average values of the erosion rate density distribution plotted at various span locations corresponding to the different mass flow rates of the sand particles on the pressure side of the blade

Figure 13 and 14 shows the effect of particle size (d_P) and particle's mass flow rate (m_P) on the overall performance of the compressor in terms of pressure ratio. It could be seen that pressure decreases with the with the increase in the values of both parameters i.e. particle size (d_P) and particle's mass flow rate (m_P) corresponding to same values of the air flow rate. This shows that air with sand particles will increase the required power to run the compressor at the same flow rate of the air.

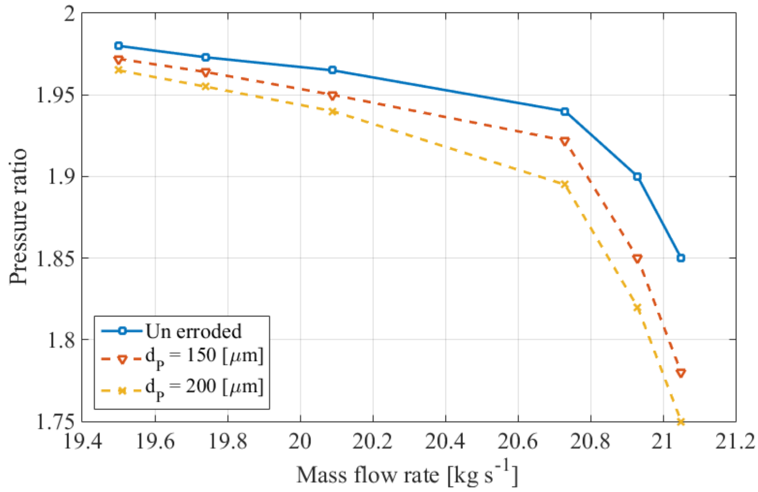

Figure 13: Variation of the pressure ration with mass flow rate of air corresponding to the different particle sizes

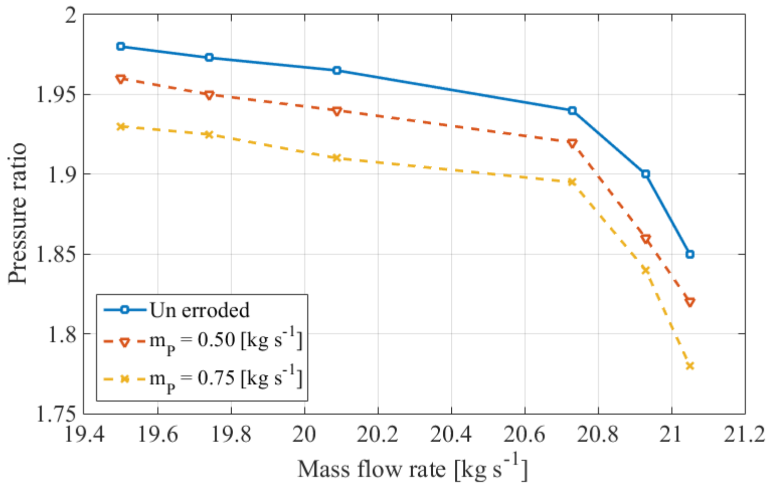

Figure 14: Variation of the pressure ration with mass flow rate of air corresponding to the different particle flow rates

Acknowledgements

This paper was funded by the Deanship of Scientific Research (DSR) at King Abdulaziz University, Jeddah. The investigators, therefore, acknowledge with thanks DSR for technical and financial support.

References

[1]. Reid L, Moore RD, "Design and Overall Performance of Four Highly-Loaded, High-Speed Inlet Stages for an advance, High-Pressure-Ratio Core Compressor," NASA TP-1337, Lewis Research Center, Cleveland, Ohio, Oct. 1978.

[2]. Suzuki M, Inaba K, Yamamoto M, "Numerical simulation of sand erosion phenomena in rotor/stator interaction of compressor," Journal of Thermal Science, Vol. 17, No. 2, 2008, pp. 125-133.

[3]. Suzuki M, Yamamoto M, "Numerical Simulation of Sand Erosion Phenomena in a Single-Stage Axial Compressor," Journal of Fluid Science and Technology, Vol. 6, No. 1, 2011, pp. 98–113.

[4]. Elfeki S, Tabakoff W, "Erosion Study of Radial Flow Compressor with Splitters," Journal of Turbomachinery, Vol. 109, No. 1, 2009, pp. 62.

[5]. Litt JS, Simon DL, "Toward a Real-Time Measurement-Based System for Estimation of Helicopter Engine Degradation Due to Compressor Erosion," Journal of the American Helicopter Society, Vol. 54, No. 1, 2009, pp.012008-1-012008-8.

[6]. Hamed A, Tabakoff W, Singh D, "Modeling of compressor performance deterioration due to erosion," Journal of the American Helicopter Society, Vol. 4, No. 4, 1998, pp. 243-248.

[7]. Tabakoff W, Lakshminarasimha AN, Pasin M, "Simulation of Compressor Performance Deterioration Due to Erosion," Journal of Turbomachinery, Vol. 112, No. 1, 2008, p. 78.

[8]. Hutchings I, "Mechanical and metallurgical aspects of the erosion of metals," Wear, 1979, pp. 393-427.

[9]. Finnie I, "Some observations on the erosion of ductile metals," Wear, 1972, pp. 81-90.

[10]. ANSYS CFX, “CFX-Pre user’s guide release 16.0.” Ansys Inc., Canonsburg, 2015.

[11]. Saeed M, Man-Hoe K, “Airborne Wind Turbine Shell Behavior Prediction Under Various Wind Conditions Using Strongly Coupled Fluid Structure Interaction Formulation,” Energy Conversion and Management. Vol. 120, 2016, pp. 217-228.